| **IET Optoelectronics**

IET The Institution of Engineering and Technology WILEY

ORIGINAL RESEARCH

Multispectral Optical camera communication links based on spectral signature multiplexing

Daniel Moreno[1] | **Victor Guerra**[2] | **Julio Rufo**[3] | **Jose Rabadan**[1] |
Rafael Perez-Jimenez[1]

[1]Institute for Technological Development and Innovation in Communications (IDeTIC), Universidad de las Palmas de Gran Canaria (ULPGC), Las Palmas de Gran Canaria, Las Palmas, Spain

[2]Pi Lighting Sarl, Sion, Valais, Switzerland

[3]Higher Polytechnic School of Engineering and Technology, Universidad de La Laguna (ULL), San Cristóbal de La Laguna, Santa Cruz de Tenerife, Spain

Correspondence

Daniel Moreno.
Email: daniel.moreno@ulpgc.es

Abstract

Optical camera communication is foreseen to have an essential role in future systems requiring wireless communication capability. In this regard, high-spectral-resolution cameras, such as multispectral (MS) cameras, present specific characteristics that can be exploited to provide new features to optical camera communication links. Using the MS cameras' features to take advantage of the light-emitting diode (LED) behaviour in a novel communication scheme is focussed. Notably, LED spectral response curves are different when their temperature changes. Therefore, these differences can be detected based on the MS cameras' spectral resolution. Thus, more than one communication channel can be attained using the same LED device since the camera can distinguish the different LED spectral signatures. This new approach is analysed in this work, including some equalisation techniques applied to the channel matrix in the receiver to improve the extraction of the transmitted signal reducing the inter-channel interference. For the specific MS camera employed in the experiments, up to two distinct channels could be obtained with the same transmitter at different temperatures, getting a bit error rate below the forward error correction limit. However, obtaining satisfactory results is highly dependent on the variation that temperature causes in the spectral signatures of the LEDs, so further experiments are recommended in future work with different devices.

KEYWORDS

cameras, light emitting diodes, multiplexing, optical communication

1 | INTRODUCTION

Optical camera communication (OCC) has been gaining much attention owing to the widely used types of cameras featured in electronic devices, vehicles, surveillance, and healthcare systems. In addition, the pervasiveness of these devices and the emerging developments in image sensors have prompted this technology for research purposes [1]. Besides, OCC has undergone a revolution in the scientific community over the past decades for its promising immediate applications to the market compared with visible light communication (VLC) systems, which lack commercially available off-the-shelf (COTS)

devices. As a result, new modulation/demodulation approaches and diverse transmitters and cameras have been the subject of recent research. For example, Shiraki *et al.* reported on a demodulation scheme based on a Gaussian-mixture model for an OCC system to obtain the channel states without using synchronization devices in the transmitters [2]. Besides, Hu *et al.* designed an light-emitting diode (LED)-to-camera communication system using colour shift keying (CSK) modulation. The authors evaluated the performance of multiple camera sensors embedded in smartphones achieving low error symbol rates addressing common issues, such as colour flicker, inter-frame data loss, and receiver (RX) diversity [3].

Additionally, recent studies utilised neural-network-based approaches to decode information. For instance, Chow *et al.* used a rolling shutter image sensor and an LED light panel for an OCC system. Frame-averaging background removal technique, Z-score normalisation, and neural network were used to achieve non-linear distortion mitigation and satisfactory bit error rate (BER) performance in high inter-symbol interference situations [4]. Furthermore, Tsai *et al.* proposed a pixel-row-per-bit-based neural network to decode data produced by an optical-diffusing-fibre (ODF) transmitter in an OCC link. The authors demonstrated that the proposed algorithm enhanced the BER compared to traditional artificial neural network (ANN) [5].

In spite of the growing body of literature on OCC, the technology's potential still needs to be fully explored, particularly beyond the application of traditional cameras. For instance, several researchers put forward high-speed cameras to boost the bit rate, as in Arai *et al.*'s work, where the authors proposed a hierarchical transmission scheme based on a two-dimensional fast Haar wavelet transform. Thus, data detection is ensured when the camera is distant from the LED emitter [6]. Moreover, Iwase *et al.* proposed a lighting pattern recognition strategy from a pattern-mixed image, adjusting the data rate to the same receiver frame rate and decreasing flickering through 8b/10b encoding [7]. Alternatively, the behaviour of LEDs as optical data transmitters has also been analysed. In particular, temperature-related changes in the LED spectral properties are widely recognized to have a negative impact on communication performance if they are not taken into consideration during the data reception [8, 9].

This paper presents a communication scheme using LEDs as transmitters and a multispectral (MS) camera as a RX. The multiple camera bands provide a higher spectral resolution, permitting the distinction of optical signals with wavelengths. In addition, the LED spectral shift caused by thermal variations is taken advantage of. Given that the spectral signatures of the LEDs vary with temperature modifications, these changes are captured by a high-spectral-resolution camera. The spectral variations will be used to differentiate the LED's transmissions at different temperatures. As a result, new communication channels can be established using the same type of device because the temperature affects the LED's spectral response curves.

To achieve these channels, traditional linear methods have been chosen. This approach may be compared to previous methods that used clustering to obtain communication channels, which have been shown to have better performance than traditional linear methods such as zero-forcing (ZF) equalisation [10]. However, this study provides a deeper analysis of ZF and minimum mean square error (MMSE) equalisation, demonstrating that it can also produce satisfactory results. Additionally, the comparison of this approach to previous methods can provide valuable insight for the research community. Our submission includes experimental results and further analysis to validate the proposed method.

This paper takes a new look at OCC systems by employing an MS camera and thermally induced spectral changes on LEDs. A novel approach is presented, exploring the possibility of adopting a spectral signature multiplexing based on temperature. It is an innovative method as an alternative to wavelength division multiplexing (WDM), which is detailed in the following sections. Consequently, this study aims to assess the performance of this new proposal by making use of the characteristics of MS cameras that allow discriminating the spectral responses of LEDs at different temperatures.

This paper is divided into six sections. Section 2 provides a brief overview of OCC and discusses the benefits of utilising an MS camera as a receiver in OCC. Section 3 explores the effect of temperature on LEDs. Section 4 outlines the procedures and techniques used to perform the experiments. Section 5 presents the results obtained from the methodology implemented. Finally, Section 6 offers some concluding remarks.

2 | MULTISPECTRAL CAMERA COMMUNICATION

Optical camera communication uses cameras or image sensors to capture optical signals, unlike VLC systems that employ photodiodes. Therefore, this technology takes advantage of the cameras in most electronic devices, making it possible to implement this system without needing additional or modified hardware. Nonetheless, the fact that these cameras are not optimised for communications hinders the bit rate that can be achieved in OCC as it depends on the pixel clock and the scanning method, thereby making this technology oriented to low data rate links [11].

Therefore, one of the main challenges in OCC is data rate improvement, so recent developments have concentrated on proposing different schemes and techniques in this regard. Younus *et al.* implemented an ANN equaliser to reduce intersymbol interference and enhance the data rate. The authors trained the ANN once for several exposure times and stored it in a look-up table [12]. Nonetheless, their result needed to provide more robustness to high exposure time, limiting their usability in applications where visualisation and data gathering were needed. This limitation was overcome in ref. [13] using a convolutional autoencoder for improving signal quality, allowing exposure times up to 7 times greater than the symbol period and with a more computationally efficient architecture than in ref. [12]. Huang *et al.* proposed a real-time OCC system based on colour-intensity modulation multi-input-multi-output (CIM-MIMO). They created a high-dimensional signal constellation and parallel communication channels using spatial, colour, and intensity dimensions to boost data rate and improve the BER performance [14].

As OCC can use the entire light spectrum (ultraviolet, visible light, and infrared), not only visible light, high-spectral-resolution cameras, such as MS or hyperspectral cameras, can provide multiple-wavelength sensitivity utilising one device. Hence, due to the filters centred on different wavelengths that this type of camera has, the application of WDM or MIMO techniques could be simplified.

Moreover, considering the temperature effects on LEDs, which modify their spectral behaviour, MS cameras can turn this a priori detrimental factor into an advantage. The high spectral resolution of those devices would detect multiple signals from the same light source at various temperatures as a function of the band number and their bandwidth [15]. This issue is crucial in this research and will be thoroughly addressed in Section 3.

To the best of the authors' knowledge, the employment of MS cameras as receivers in an OCC system has yet to be exploited. Therefore, multispectral camera communication (MCC) is a field that can be explored and OCC performance is improved because of the natural characteristics of this kind of camera.

For the optical wireless communication's channel modelling, Equation (1) represents the OCC system's received power.

$$P_{rx} = P_{tx}R(\theta, \phi)\frac{A_{lens}}{d^2}\cos(\Psi), \tag{1}$$

where P_{tx} is the transmitted power, $R(\theta, \phi)$ is the source's radiation pattern at elevation θ and azimuth ϕ, A_{lens} is the main lens' cross-section, d is the link range, and Ψ is the impact angle. Considering the image-forming optics theory inherent when employing cameras as receivers for communication, it is demonstrated that the pixel power does not depend on the distance if the LED's projected size on the image sensor is greater than one pixel [16].

$$A_{proj} = \frac{N_x N_y}{FOV_x FOV_y}\frac{A_{tx}}{d^2}, \tag{2}$$

where A_{proj} is the projected number of pixels of the optical emitter on the sensor, N_x and N_y define the sensor's pixel resolution, FOV_x and FOV_y are the camera's horizontal and vertical fields of view, respectively, and A_{tx} is the transmitter's effective area (from the receiver's viewpoint). It can be seen from these equations that P_{rx} and A_{proj} decrease with increasing distance (constant power density on the image sensor). Thus, the received optical power at each pixel is expressed in Equation (3) by combining Equations (1) and (2).

$$P_{px} = P_{tx}R(\theta, \phi)\frac{A_{lens}}{A_{tx}}\frac{FOV_x FOV_y}{N_x N_y}A_{px}\cos(\Psi), \tag{3}$$

where P_{px} is the pixel power (in watts) and A_{px} is the pixel area.

Moreover, channel compensation is critical in any system subject to inter-channel interference (ICI). Several techniques aim to alleviate ICI, such as MIMO, WDM, and CSK, which require an equalisation stage to minimise the interference in VLC systems. ZF and MMSE equalisers are the usual algorithms applied to equalise [17–19].

On the one hand, ZF equalisers are linear algorithms that minimise ICI to zero in noiseless situations. Channel matrices in MCC are formed by the received spectral signatures of the transmitters. Since the channel matrices are likely to be non-square because the transmitters and the camera's number of bands may differ, the Moore-Penrose pseudo-inverse ($\mathbf{W}$) can be applied to determine the inverse matrix (Equation 4), thereby estimating the received signal.

$$\mathbf{W}_{ZF} = \mathbf{H}^T\left(\mathbf{H} \cdot \mathbf{H}^T\right)^{-1}, \tag{4}$$

where $\mathbf{H}$ is the channel matrix and T indicates transposition.

On the other hand, in scenarios where the signal-to-noise ratio (SNR) is not high and ZF equalisers are limited, MMSE equalisers would be more suitable. Equation (5) shows the calculation of the matrix that is used to approximate the received signal to the transmitted signal.

$$\mathbf{W}_{MMSE} = \mathbf{H}^T\left(\mathbf{H} \cdot \mathbf{H}^T + \frac{1}{SNR} \cdot \mathbf{I}\right)^{-1}, \tag{5}$$

where $\mathbf{I}$ is the identity matrix. It is straightforward to verify from Equation (5) that $\mathbf{W}_{ZF}$ (Equation 4) and $\mathbf{W}_{MMSE}$ are consistent for high SNR values.

Moreover, the received signal y can be expressed as follows:

$$y = \mathbf{H} \cdot x + n, \tag{6}$$

where x is the transmitted signal and n is additive white Gaussian noise (AWGN). After calculating the compensation matrix $\mathbf{W}$, integrating the linear compensation to Equation (6) estimates the transmitted signal (Equation 7).

$$\hat{x} = \mathbf{W} \cdot (\mathbf{H} \cdot x + n) \tag{7}$$

It is worth noting that $\mathbf{W}$'s components will be susceptible to AWGN, disregarding the calculation technique used. The compensation approach will thus be flawed, necessitating an evaluation of its performance. In this sense, calculating the condition number of the channel matrix is proposed as an option to assess performance [15] (Equation 8). The transmitted signal is more accurately estimated by well-conditioned matrices (values near to one) than by ill-conditioned ones (values much higher than one).

$$\text{cond}(\mathbf{H}) = \|\mathbf{H}\| \cdot \|\mathbf{H}^{-1}\| \tag{8}$$

3 | THERMAL EFFECTS ON LED DEVICES

In the literature, LED temperature effects have been widely addressed. Some of the main aspects discussed are the impact that changes in the p-n junction temperature cause on the efficiency and the spectral.

Equation (9) is commonly used to model the relationship between the semiconductor material's energy gap and the junction temperature [20]. Accordingly, the energy gap usually

decreases as the temperature rises. In addition, a change in LED emission is caused as the wavelength increases with temperature due to the Planck-Einstein connection (Equation 10).

$$E_g = E_0 - \frac{\alpha T^2}{T + \beta}, \tag{9}$$

where T is temperature, E_0 is energy gap at 0 K temperature condition, and α and β are semiconductor-dependent constants, which are empirically determined.

$$E_g = hf = \frac{hc}{\lambda}, \tag{10}$$

where h is Planck's constant, f is frequency, c is the speed of light in vacuum, and λ is wavelength.

On the other hand, several investigations have studied the impact of temperature on photometric parameters. For instance, optical parameters of surface mount device LEDs were determined under different temperature conditions in ref. [21], revealing a predictable red shift of the peak wavelength when the temperature grew. Likewise, temperature influenced the devices' intensity, spectral width, and colour coordinate shifts. Furthermore, other parameters were examined in [22]. Namely, the LED's luminous flux and efficacy were estimated at different operating conditions. The authors found the optimised conditions of the light sources considering that the aforementioned parameters decrease as junction temperature increases.

Many studies have been conducted on LED lifetime by the accelerated ageing test. These studies conducted tests that subjected LEDs to the leading causes affecting their behaviour, that is, temperature and current through the LED. Most recent evidence shows that luminous flux, colour changes, and lifetime are sensitive to thermal effects, and the current stress degrades the LEDs more than the thermal stress [23–25].

This study suggests utilising an MS camera in light of the thermal impact indicated earlier. Remarkably, it is proposed to capture the spectral shifts caused by temperature.

Considering the temperature effects mentioned above, this work proposes taking advantage of the thermal impact on LEDs, especially those concerning spectral changes, to utilise an MS camera that captures the variation. Therefore, applying a regulated temperature to the transmitter is conceivable to have the same LED with a distinct spectral response curve. Consequently, using an MS camera as a receiver in an OCC link, these spectral changes could be exploited to establish new communication channels.

4 | METHODOLOGY

The main aim of this work is to experimentally test the performance of an MS camera in a communication link (LED-to-camera). In order to exploit the high-spectral-resolution

capability of this kind of camera, LEDs of a specific wavelength have been employed at different driving currents to modify their working temperature and get different spectral signatures that the MS camera can detect.

4.1 | Experimental setup

Different types of LEDs were used as transmitters in the system. Each LED's driving current was adjusted by a circuit powered by a voltage source. In addition, the circuits were linked to a microcontroller that output a variable pulse position modulation signal based on the target temperature to be induced in the LED by the Joule heating effect. Finally, the microcontroller devices and the control PC were paired to send the transmitted data over the serial port.

Additionally, the PC connected to the MS camera managed the image acquisition procedure through Ethernet. It was necessary to use a diffuser between the LEDs and the camera to mix the light beams and prevent pixel saturation. Furthermore, the entire system was set inside a dark room to minimise the influence of background light. Lastly, all the operations were coordinated using a Python-based automation script that enabled communication between the microcontroller devices and the camera.

4.2 | Description of procedures

The basic concept of the experiment was to use groups of the same LED model and change their p-n junction temperature by the Joule effect to obtain different spectral signatures. Since each LED possessed a particular spectral response curve, an MS camera could capture it. Hence, the LEDs were set with distinct pulse-width modulation (PWM) duty cycle (DC) values to have those different signatures. Thus, the higher the DC value, the higher the junction temperature. Because one of the purposes of the experiment was to get the maximum spectral variation caused by temperature, no thermal management techniques, such as heat sinks, were used in this work as they would reduce the changes in the LED's spectral characteristics. After reaching the target temperature, the data transmission started, the camera captured the images, and finally, the system's performance was evaluated. In light of the explanation above, Figure 1 outlines the three main phases of the experiment.

In the first phase, several LED p-n junction temperatures must be achieved. Therefore, the LEDs were set with 30% and 70% of DC values when using two transmitters and 30%, 50%, and 70% when using three transmitters. The frequency of the PWM was set to 5 Hz (bit time of 200 ms). In order to reach the thermal steady state on the LEDs, the transmitters were set to an idle state for 5 min before sending data because no external thermal management technique was applied to stabilise the temperature. It consisted of keeping the LEDs sending a binary zero with the corresponding DC.
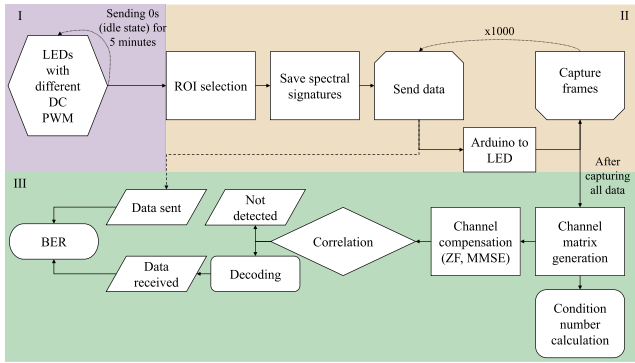
FIGURE 1 Flowchart of the procedures. The methodology is split into three phases. Phase I: LED temperature stabilisation. Phase II: transmit-receive process. Phase III: system performance assessment. LED, light-emitting diode.

During the second phase, the region of interest, where the light beams of the LEDs were mixed, was selected. Then, the channel matrix was estimated by capturing the spectral responses of each LED. After that, the transmission began. On the other hand, data transmission was based on the following steps. First, a list of 1000 eight-bit pseudo-random integers was generated for each transmitter. Next, the elements of each list were sent to the microcontroller devices in byte format. However, the generated bit sequence was 8b/10b encoded in the microcontroller part. Due to the sensitivity of the spectral signature to temperature, it was essential to avoid long sequences of "1" or "0". Therefore, the applied encoding allowed a header comprising non-consecutive "0" and "1". Likewise, the same header was added after the payload to improve the frame-detection process. Figure 2 depicts the structure of the bit stream.

Regarding the MS camera, it has eight narrow bands whose centre wavelengths are, from band 1 to band 8: 424, 464, 504, 544, 573, 614, 656, and 699 nm, respectively. Besides, it possesses one panchromatic band that covers the wavelength range from 400 to 800 nm (band 9). The MS camera's frame rate was set to 50 frames per second (fps) and a working mode to global shutter. These parameters would allow capturing every 20 ms, so, as the bit time was 200 ms, it permitted 10 samples per bit. Although the orchestration script synchronized transmission and data capture, a guard period was added before and after data transmission to ensure that the whole bit stream (header + payload + footer) was captured. Those frames were stored in a ring buffer and saved individually per every data sent. As for the exposure, the aperture setting was f/2.4, the maximum allowed by the lens, and the exposure time varied according to the LEDs used (Table 1) with the purpose of not saturating the camera with the signals.

Finally, the third phase evaluated the system performance once all the data were taken. It began with the generation of the channel matrix. The spectral signatures of each LED were normalised by their maximum values and added to the matrix so that it had one signature per row. Alternatively, the condition number of the matrix was calculated as a metric of its performance. Following this, the channel matrix was compensated by
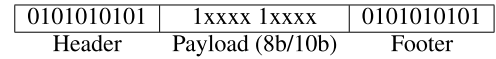
0101010101	1xxxx 1xxxx	0101010101
Header	Payload (8b/10b)	Footer

FIGURE 2 Packet structure of the bit streams.

TABLE 1 Key parameters of the experiment.

Parameter	Value
Transmitter	
Light sources	Kingbright L-53SRC-C (Red)
	Kingbright L-154A4SUREQBFZGEW (Green, Blue)
Dominant wavelengths [nm]	660 (Red), 520 (Green), 460 (Blue)
Control device	Arduino UNO
Receiver	
Camera	SILIOS Technologies CMS-C1-C-EVR1M-GigE
Resolution [px]	1280×1024 (raw image)
	426×339 (multispectral images)
Exposure time [ms]	20 (Red), 6.5 (Green), 0.25 (Blue)
Aperture	f/2.4
Frame rate [fps]	50
Shutter mode	Global shutter
Bit stream	
Coding	8b/10b
Modulation	VPPM
Bit time [ms]	200
Duty cycle	30%, 50%, 70%
Bits	Header: 10, Payload: 8, Footer: 10

applying ZF and MMSE algorithms. At this point, the mixed signals were consequently split into two (or three) signals. The resulting signals were then correlated with a matrix comprising all available transmitted signals.

Given that the length of the transmitted signal (header + payload + footer) was shorter than the length of the received signal because the latter included extra frames to avoid missing information, the correlation was performed by traversing the template signals through the received signal. As soon as the correlation had been done, the maximum value was then taken. Before decoding the signal, in order to prevent getting a large number of bit errors, a correlation threshold was established. The bit stream was deemed undetected if the maximum coefficient was less than the threshold. Otherwise, if it was greater than the threshold, the received signal was decoded and compared to the sent signal obtaining the BER. The procedure was replicated for several thresholds ranging from 0 to 0.95. Lastly, the whole process was repeated for each LED group. Table 1 summarises the experiment key parameters.

5 | RESULTS

Table 2 shows the condition numbers of all the matrices used in this study. It is divided into two columns corresponding to the number of transmitters, which in turn are subdivided into three columns corresponding to the red-green-blue LEDs. It is apparent that the red LEDs performed the lowest values, revealing that their spectral signatures are the most distinguishable. On the contrary, the green and the blue LEDs obtained similar results. It is mathematically demonstrated that as the condition number approaches infinity when a spectral response curve is close to a linear combination of others. Consequently, matrices comprising the LED spectral signatures at different temperatures whose variability from each other is not significant would be worse conditioned than those matrices formed by the spectral signatures of LEDs with substantial variability.

Figure 3 depicts the spectral signatures of the three LEDs (red, green, and blue) at different temperatures (several DC values). The x-axis represents the spectral bands, whereas the y-axis represents the normalised camera level. It can be seen that the spectral signatures of the red LEDs showed the highest variability from each other, while the green and the blue LEDs presented a higher similarity, respectively.

The system performance for two and three LED emitters is illustrated in Figures 4 and 5. They show the BER and the undetected bit streams depending on the imposed correlation threshold. A ZF algorithm was employed for channel compensation. The results from the MMSE equaliser were left out in this contribution as they performed similarly to ZF because of the high link SNR.

As expected, the red LEDs produced the best results in terms of performance examination, followed by the green and blue LEDs. For the LEDs at 30% and 70%, the BER of the red light sources was roughly 10^{-2} from thresholds of 0–0.25 as shown in Figure 4a. Additionally, from the detection thresholds of 0.5 and 0.6, the BER was below the forward error correction (FEC) limit ($3.8 \cdot 10^{-3}$) for the LEDs at 30% and 70%, respectively. Specifically, a BER slightly less than $3.5 \cdot 10^{-3}$ was achieved, along with approximately 3% of the bit streams not detected. Finally, none of the bit streams were detected for the LEDs from the thresholds of 0.85 and 0.9 at 30% and 70%, respectively.

Figure 4b depicts the green LEDs curves. It can be seen that the transmitter at 30% obtained a BER of approximately $4.7 \cdot 10^{-2}$ for the minimum threshold values. From the thresholds greater than 0.75, this LED achieved a BER of $2.5 \cdot 10^{-3}$, missing 17% of the bit streams. The LED at 70% outperformed its counterpart getting a BER of $3.2 \cdot 10^{-2}$ for the

lower threshold values. The BER was below the FEC limit when the thresholds exceeded 0.7. Its most remarkable outcome was a BER of $3.7 \cdot 10^{-3}$ and about 10% of the bit streams undetected. At a threshold of 0.95, the bulk of bit streams of the LED at 30% was not detected, while about 35% of the bit streams were missed for the LED at 70%.

It can be noted from Figure 4c that the blue LEDs failed to get a BER below the FEC limit. For the LED at 30%, a BER of $3.3 \cdot 10^{-3}$ was achieved, but discarding slightly more than 40% of the bit streams at a threshold of 0.85. For the LED at 70%, a BER of approximately 10^{-4} was reached, not detecting
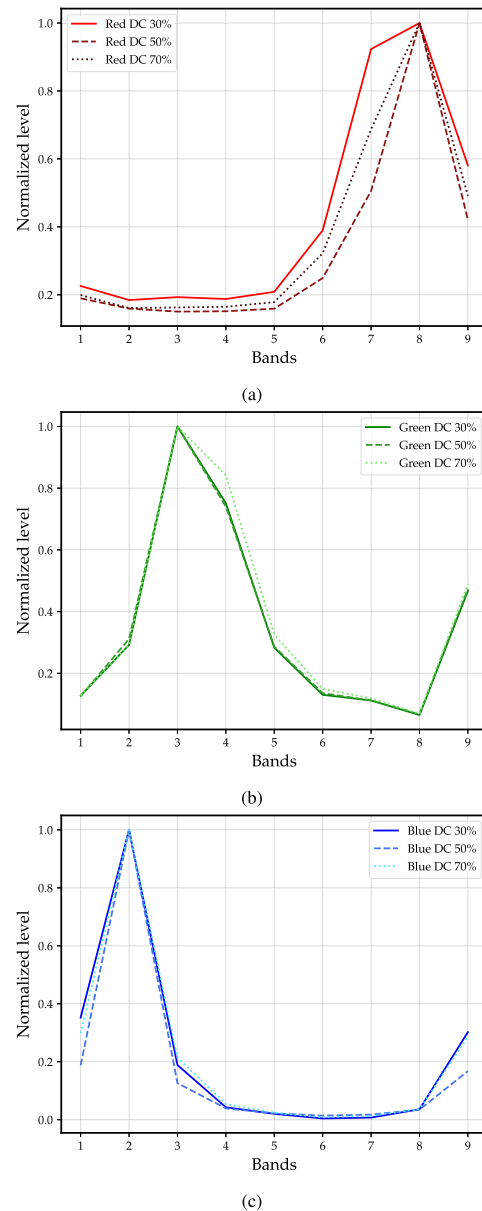

(a)

(b)

(c)

FIGURE 3 Spectral response curves of the three LEDs used in this study at different temperatures. (a) Red LEDs, (b) green LEDs, and (c) blue LEDs. Solid, dashed, and dotted lines correspond to the LEDs working at 30%, 50%, and 70% duty cycle (DC) values, respectively. LED, light-emitting diode.

TABLE 2 Channel matrices condition numbers.

Condition number (dB)	2 TXs			3 TXs		
	R	G	B	R	G	B
	24.10	31.29	31.18	42.80	45.48	50.60

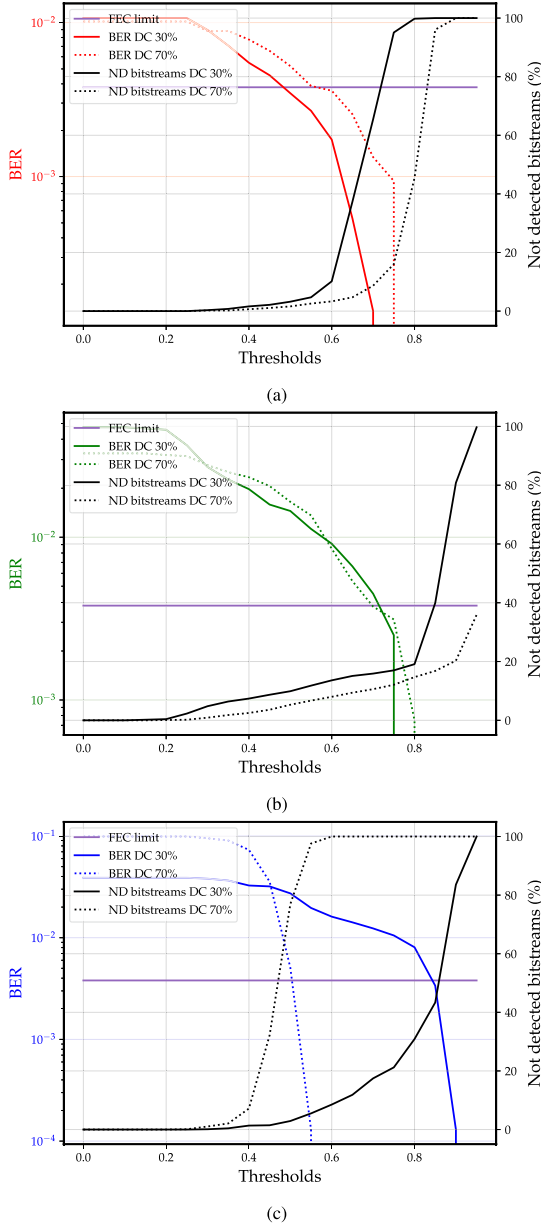Abbreviation: TXs, diverse transmitters.

FIGURE 4 Bit error rate (BER) and undetected bit streams at various correlation thresholds corresponding to the (a) red, (b) green, and (c) blue LED pairs. Solid and dotted lines correspond to the LEDs working at 30% and 70% duty cycle (DC) values, respectively. LED, light-emitting diode.

FIGURE 5 Bit error rate (BER) and undetected bit streams at various correlation thresholds corresponding to the (a) red, (b) green, and (c) blue LED trios. Solid, dashed, and dotted lines correspond to the LEDs working at 30%, 50%, and 70% duty cycle (DC) values, respectively. LED, light-emitting diode.

more than 90% of the bit streams at a threshold of 0.55. Table 3 outlines the aforementioned results.

Regarding the three-transmitter case (Figure 5), none of the colours could perform satisfactorily with most of their BER values above the limit.

The quality of the above results depended mainly on the separation by channel compensation of the mixed signals. Figure 6 pinpoints an example of the transmission of the red LEDs. The first row depicts the received signal, that is, the mixed signals of both LEDs. In order to ease the visualisation, only the panchromatic band was shown. The second and third rows show the separated signal after compensation and the data sent corresponding to the LEDs at DC 30% and 70%,
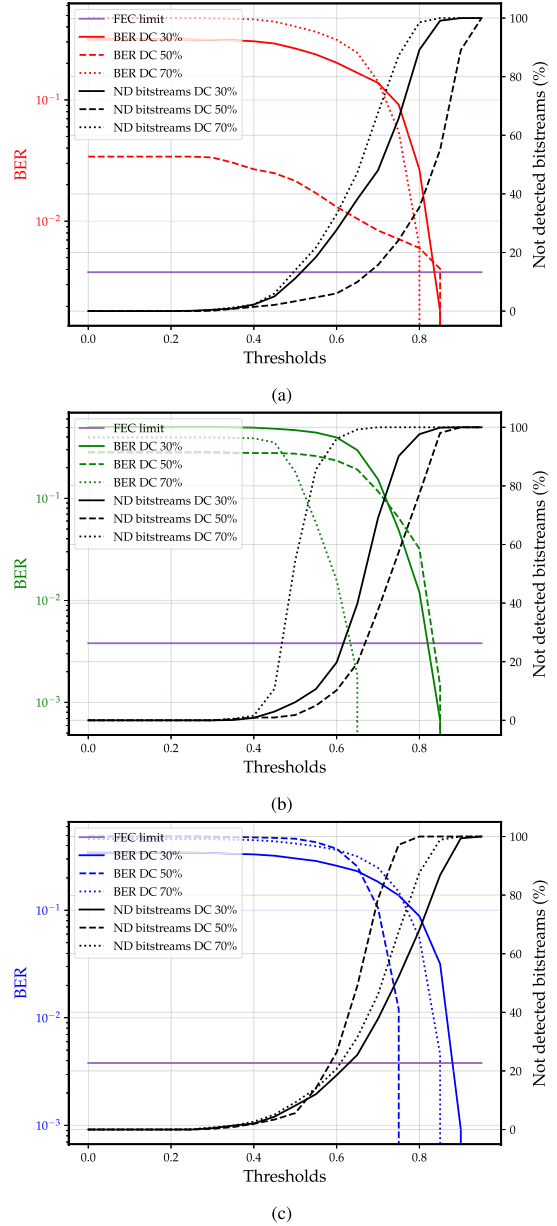
TABLE 3 Comparison of LED performance.

LEDs	DC	BER below FEC limit	Undetected bit streams	Threshold
Red	30%	$3.48 \cdot 10^{-3}$	3.21%	0.50
	70%	$3.61 \cdot 10^{-3}$	3.32%	0.60
Green	30%	$2.50 \cdot 10^{-3}$	17.00%	0.75
	70%	$3.75 \cdot 10^{-3}$	10.60%	0.70
Blue	30%	$3.38 \cdot 10^{-3}$	43.35%	0.85
	70%	$1.30 \cdot 10^{-4}$	97.61%	0.55

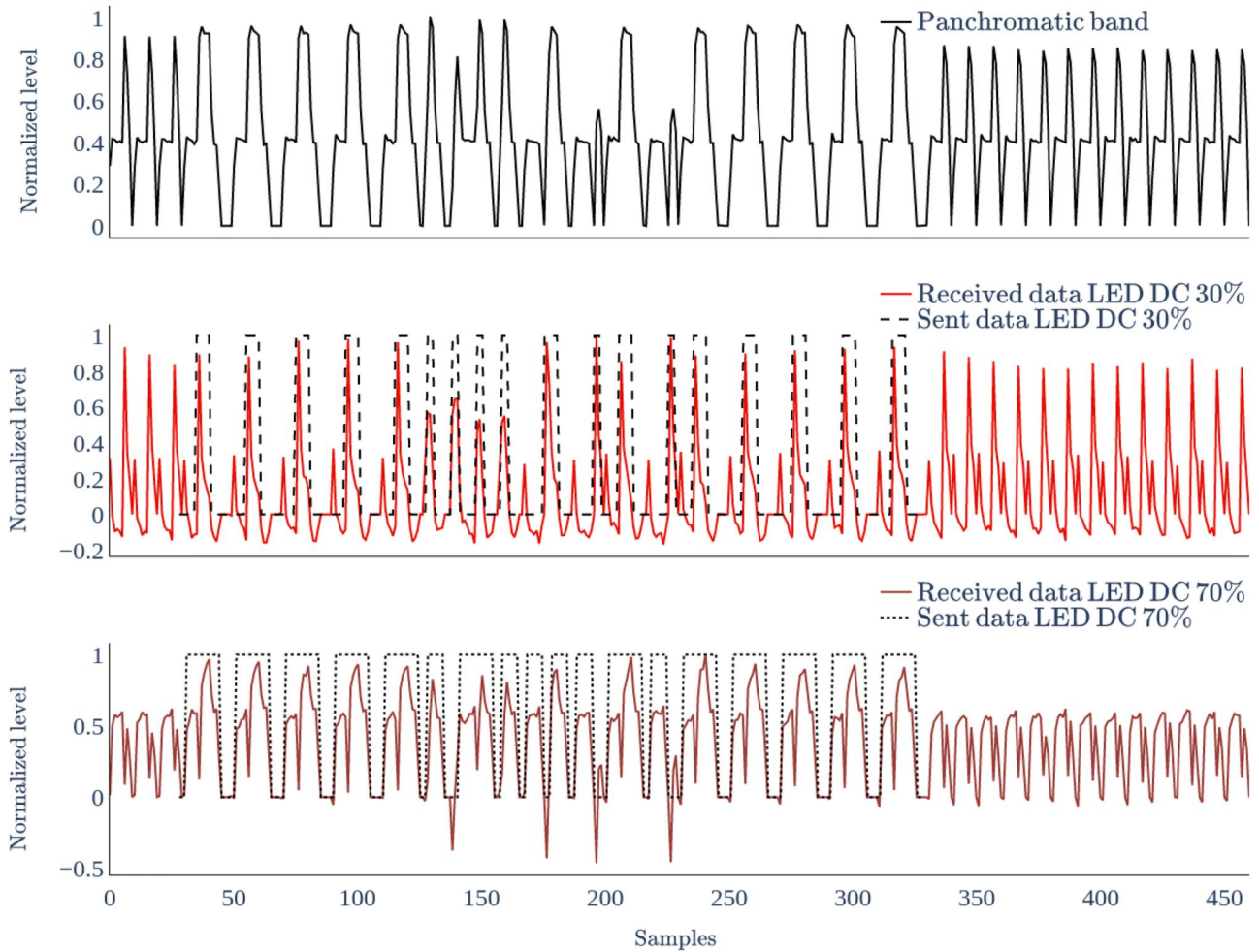Abbrevition: LED, light-emitting diode.

FIGURE 6 Example of transmission of the red LEDs. The first row shows the mixed signal of the LEDs received by the camera. The second and the third rows depict the signals after compensation of the LEDs at 30% and 70%, respectively. The sent data are superimposed for both LEDs.

respectively. In Figure 6, LED 1 (DC 30%) sent a decimal 226 (1110 0010) and LED 2 (DC 70%) sent a decimal 123 (0111 1011). Note that the bit streams show the data after the 8b/10b encoding (LED 1: 11110 10010, LED 2: 10111 11011). It can be seen that the bit streams started at approximately sample 28 and finished at sample 328. For the rest of the samples, the LEDs were in an idle state. It is remarkable to note that, although both signals interfere, the decoding process was successful. Because of that interference, when LED 1 had a peak, LED 2 tended to have a trough and vice versa (for instance, see the peaks between the "1" of the header in LED 1). In the cases where the decoding was not satisfactory, the co-channel interference mentioned above was higher than the one shown in this example, resulting in more bit errors.

6 | CONCLUSIONS

An OCC communication system was conducted in this research employing an MS camera as the data receiver. Furthermore, the spectral features of the light sources employed as transmitters were altered by modifying their p-n

junction temperature. Thus, the same LED model would provide different spectral behaviours, which the MS camera would exploit. The LED temperatures were varied because of the Joule effect by supplying various driving currents to the LEDs. No heat sink was used in this work since it would have reduced the thermally induced spectral variation of the LEDs. Groups of LEDs with different dominant wavelengths have been used, and their performance has been analysed.

The strong point of this contribution lies in attaining multiple channels from the same LED by altering its temperature. A high-spectral-resolution camera, namely an MS camera, makes it possible to capture the slight dissimilarities in the LED's spectral signatures. The findings of this work demonstrate that for certain LEDs whose spectral properties are significantly affected by heat fluctuations in their p-n junction temperature, the BER below the FEC limit can be attained. It is worthwhile noting that in situations where the bit streams were not detected, a re-transmission strategy could be used.

Conversely, the green/blue LEDs' results were below expectations. The foremost factor of this poor performance is the temperature repercussion on those transmitter devices. Notably, the green and the blue devices were less thermally

impacted than the red LEDs, which peak wavelengths were noticeably red-shifted. Besides, it was evident from the condition number of the channel matrices that the ill-conditioned matrices obtained the most unsatisfactory performance. Consequently, the results of this study support the idea that utilising light sources whose spectral features are further influenced by temperature changes would enhance the experiment's success. Nevertheless, in those cases where the optical emitters are employed for illumination and communication, a compromise between the level of spectral changes and the efficiency drop resulting from thermal effects must be taken into account.

Moreover, the performance was unsuccessful when using three LEDs. There are two principal sources for this poor result. First, the slight variation in the spectral response curves brought about by changes in the LED p-n junction temperature limits the capability to obtain new communication channels. Second, the spectral resolution of the camera plays a crucial role in differentiating spectral signatures. Thus, the higher the number of bands and the thinner their width, the higher the resolution. Having considered those aspects, it could be seen in Section 5 by observing the spectral signatures and the condition number for the case of three transmitters that the signals did not present a considerable difference that would make them distinguishable for the employed camera.

An important implication of this research is the increase in the number of channels that can be achieved from a single transmitter by taking advantage of the impact of temperature.

More broadly, light sources with different peak wavelengths can be employed. Accordingly, using the method implemented in this research, the spectral bands of the camera with a specific centre wavelength would facilitate the separation of the signals. Furthermore, the potential for utilising the temperature impact on LEDs is an ongoing spur for further experimental studies. For example, future work should address the analysis of different LEDs (the same model and distinct ones) to assess the value of each device in this technique.

AUTHOR CONTRIBUTION

Daniel Moreno: Data curation, Investigation, Methodology, Software, Visualisation, Writing – original draft. **Victor Guerra:** Data curation, Formal analysis, Software, Validation, Writing – original draft. **Julio Rufo:** Conceptualisation, Supervision, Validation, Writing – review and editing. **Jose Rabadan:** Project administration, Resources, Supervision, Writing – review and editing. **Rafael Perez-Jimenez:** Funding acquisition, Project administration, Supervision, Writing – review and editing.

ACKNOWLEDGMENTS

CONFLICT OF INTEREST STATEMENT

The authors declare no conflict of interest.

DATA AVAILABILITY STATEMENT

The data that support the findings of this study are available from the corresponding author upon reasonable request.

ORCID

Daniel Moreno 🄳 https://orcid.org/0000-0003-1336-7365
Rafael Perez-Jimenez 🄳 https://orcid.org/0000-0002-8849-592X

REFERENCES

1. Chowdhury, M.Z., et al.: The role of optical wireless communication technologies in 5G/6G and IoT solutions: prospects, directions, and challenges. Appl. Sci. 9(20), 4367 (2019). [Online]. Available:. https://doi.org/10.3390/app9204367 https://www.mdpi.com/2076-3417/9/20/4367
2. Shiraki, Y., et al.: A demodulation method using a Gaussian mixture model for unsynchronous optical camera communication with on-off keying. J. Lightwave Technol. 39(6), 1742–1755 (2021). https://doi.org/10.1109/jlt.2020.3043046
3. Hu, P., et al.: High speed LED-to-camera communication using color shift keying with flicker mitigation. IEEE Trans. Mobile Comput. 19(7), 1603–1617 (2020). https://doi.org/10.1109/tmc.2019.2913832
4. Chow, C.-W., et al.: Display light panel and rolling shutter image sensor based optical camera communication (occ) using frame-averaging background removal and neural network. J. Lightwave Technol. 39(13), 4360–4366 (2021). https://doi.org/10.1109/jlt.2021.3073656
5. Tsai, D.-C., et al.: Optical camera communication (occ) using a laser-diode coupled optical-diffusing fiber (odf) and rolling shutter image sensor. Opt Express 30(10), 16069–16077 (2022). [Online]. Available:. https://doi.org/10.1364/oe.449860 https://opg.optica.org/oe/abstract.cfm?URI=oe-30-10-16069
6. Arai, S., et al.: Experimental on hierarchical transmission scheme for visible light communication using LED traffic light and high-speed camera. In: 2007 IEEE 66th Vehicular Technology Conference, pp. 2174–2178 (2007)
7. Iwase, D., et al.: Improving communication rate of visible light communication system using high-speed camera. In: 2014 IEEE Asia Pacific Conference on Circuits and Systems (APCCAS), pp. 336–339 (2014)
8. Tugcu, E., et al.: Red-shift effect in multi-color LEDs based visible light communication. Opt Commun. 463, 125451 (2020). [Online]. Available:. https://doi.org/10.1016/j.optcom.2020.125451 https://www.sciencedirect.com/science/article/pii/S0030401820301115
9. Moreno, D., et al.: Effect of temperature on channel compensation in optical camera communication. Electronics 10(3), 262 (2021). [Online]. Available:. https://doi.org/10.3390/electronics10030262 https://www.mdpi.com/2079-9292/10/3/262
10. Moreno, D., et al.: Clustering-based data detection for spectral signature multiplexing in multispectral camera communication. Opt. Lett. 47(5), 1053–1056 (2022). [Online]. Available:. https://doi.org/10.1364/ol.449207 http://opg.optica.org/ol/abstract.cfm?URI=ol-47-5-1053
11. Cahyadi, W.A., et al.: Optical camera communications: principles, modulations, potential and challenges. Electronics 9(9), 1339 (2020). [Online]. Available:. https://doi.org/10.3390/electronics9091339 https://www.mdpi.com/2079-9292/9/9/1339
12. Younus, O.I., et al.: Data rate enhancement in optical camera communications using an artificial neural network equaliser. IEEE Access 8, 42656–42665 (2020). https://doi.org/10.1109/access.2020.2976537
13. Jurado-Verdu, C., et al.: Convolutional autoencoder for exposure effects equalization and noise mitigation in optical camera communication. Opt Express 29(15), 22973–22991 (2021). [Online]. Available:. https://doi.org/10.1364/oe.433053 http://www.opticsexpress.org/abstract.cfm?URI=oe-29-15-22973

14. Huang, W., Tian, P., Xu, Z.: Design and implementation of a real-time CIM-MIMO optical camera communication system. Opt Express 24(21), 24567–24579 (2016). [Online]. Available:. https://doi.org/10.1364/oe.24.024567 http://www.opticsexpress.org/abstract.cfm?URI=oe-24-21-24567

15. Moreno, D., et al.: Optical multispectral camera communications using LED spectral emission variations. IEEE Photon. Technol. Lett. 33(12), 591–594 (2021). https://doi.org/10.1109/lpt.2021.3078842

16. Yamazato, T., et al.: Vehicle motion and pixel illumination modeling for image sensor based visible light communication. IEEE J. Sel. Area. Commun. 33(9), 1793–1805 (2015). https://doi.org/10.1109/jsac.2015.2432511

17. Hussein, Y.S., Alias, M.Y., Abdulkafi, A.A.: On performance analysis of ls and mmse for channel estimation in vlc systems. In: 2016 IEEE 12th International Colloquium on Signal Processing its Applications (CSPA), pp. 204–209 (2016)

18. Anusree, A., Jeyachitra, R.K.: Performance analysis of a MIMO VLC (visible light communication) using different equalizers. In: 2016 International Conference on Wireless Communications, Signal Processing and Networking (WiSPNET), pp. 43–46 (2016)

19. Jha, M.K., Kumar, N., Lakshmi, Y.V.S.: NOMA MIMO visible light communication with ZF-SIC and MMSE-SIC. In: 2020 2nd PhD Colloquium on Ethically Driven Innovation and Technology for Society (PhD EDITS), pp. 1–2 (2020)

20. Varshni, Y.P.: Temperature dependence of the energy gap in semiconductors. Physica 34(1), 149–154 (1967). https://doi.org/10.1016/0031-8914(67)90062-6

21. Raypah, M.E., Devarajan, M., Sulaiman, F.: Influence of injection current and ambient temperature on intensity and wavelength of low-power SMD LED. In: 2016 IEEE 37th International Electronics Manufacturing Technology (IEMT) 18th Electronics Materials and Packaging (EMAP) Conference, pp. 1–6 (2016)

22. Raypah, M.E., et al.: Estimation of luminous flux and luminous efficacy of low-power SMD LED as a function of injection current and ambient temperature. IEEE Trans. Electron. Dev. 63(7), 2790–2795 (2016). https://doi.org/10.1109/ted.2016.2556079

23. Andonova, A., Yordanov, R., Yordanova, I.: Thermal stability analysis of power LED during aging. In: Proceedings of the 2011 34th International Spring Seminar on Electronics Technology (ISSE), pp. 274–278 (2011)

24. Chan, C.-J., et al.: Study on current and junction temperature stress aging effect for accelerated aging test of light emitting diodes. In: 2016 International Conference on Electronics Packaging (ICEP), pp. 62–65 (2016)

25. Becirovic, V., et al.: Effects on LEDs during the accelerated ageing test. In: 2019 18th International Symposium INFOTEH-JAHORINA (INFOTEH), pp. 1–6 (2019)